Fiber-Coupled Diamond Quantum Nanophotonic Interface

Michael J. Burek,[1] Charles Meuwly,[1,2] Ruffin E. Evans,[3] Mihir K. Bhaskar,[3] Alp Sipahigil,[3] Srujan Meesala,[1] Bartholomeus Machielse,[3] Denis D. Sukachev,[3,4,5] Christian T. Nguyen,[3] Jose L. Pacheco,[6] Edward Bielejec,[6] Mikhail D. Lukin,[3] and Marko Lončar[1,*]

[1]*John A. Paulson School of Engineering and Applied Sciences, Harvard University, 29 Oxford Street, Cambridge, Massachusetts 02138, USA*
[2]*École Polytechnique Fédérale de Lausanne (EPFL), CH-1015 Lausanne, Switzerland*
[3]*Department of Physics, Harvard University, 17 Oxford Street, Cambridge, Massachusetts 02138, USA*
[4]*P. N. Lebedev Physical Institute of the RAS, Moscow 119991, Russia*
[5]*Russian Quantum Center, Skolkovo, Moscow 143025, Russia*
[6]*Sandia National Laboratories, Albuquerque, New Mexico 87185, USA*

(Received 29 March 2017; revised manuscript received 27 June 2017; published 25 August 2017)

Color centers in diamond provide a promising platform for quantum optics in the solid state, with coherent optical transitions and long-lived electron and nuclear spins. Building upon recent demonstrations of nanophotonic waveguides and optical cavities in single-crystal diamond, we now demonstrate on-chip diamond nanophotonics with a high-efficiency fiber-optical interface achieving >90% power coupling at visible wavelengths. We use this approach to demonstrate a bright source of narrow-band single photons based on a silicon-vacancy color center embedded within a waveguide-coupled diamond photonic crystal cavity. Our fiber-coupled diamond quantum nanophotonic interface results in a high flux (approximately 38 kHz) of coherent single photons (near Fourier limited at <1-GHz bandwidth) into a single-mode fiber, enabling possibilities for realizing quantum networks that interface multiple emitters, both on chip and separated by long distances.

DOI: 10.1103/PhysRevApplied.8.024026

I. INTRODUCTION

Luminescent point defects ("color centers") in diamond provide a solid-state platform for the realization of scalable quantum technologies [1]. For instance, demonstrations that leverage the nitrogen-vacancy (NV) center in diamond as a spin-photon interface [2–7] have included the entanglement of two distant solid-state qubits [8] and long-distance quantum teleportation [9]. While such advances have enabled recent tests of fundamental laws of nature [10], the entanglement generation rates in these experiments are currently limited by the rate of coherent photon generation and collection. To develop a scalable architecture for the realization of quantum networks [11,12], it will ultimately be necessary to engineer efficient single-photon emission into well-defined spatiotemporal modes [13].

Towards this goal, parallel efforts in the field of diamond nanofabrication and nanophotonics have demonstrated on-chip low-loss (below 1 dB/cm) diamond waveguides and a wide range of high-quality- (Q) factor optical cavities [12,14–26]. Recently, angled-etching nanofabrication [27–30] has emerged as a scalable method for realizing nanophotonic devices from bulk single-crystal diamond substrates. Using this approach, we demonstrate high-Q-factor ($>10^5$) diamond photonic crystal cavities (PCCs) [31] operating over a wide wavelength range (visible to telecom). Monolithic diamond PCCs fabricated by angled etching are especially attractive for their compatibility with post-fabrication processing techniques necessary to stabilize implantation-defined color centers, i.e., high-temperature annealing and acid treatments [32,33]. Together, recent efforts in quantum science and nanoscale engineering of diamond have resulted in the demonstration of a solid-state single-photon switch based on a single silicon-vacancy (SiV) color center embedded in a diamond PCC, as well as observation of entanglement between two SiVs implanted in a single-diamond waveguide [12]. As diamond nanophotonics continues to enable advances in other disciplines (including nonlinear optics [34,35] and optomechanics [36,37]), the demand for scalable technology necessitates moving beyond isolated devices to fully integrated on-chip nanophotonic networks in which waveguides route photons between optical cavities [38]. Moreover, for applications involving single photons, such as quantum nonlinear optics with diamond color centers [12,22], efficient off-chip optical-coupling schemes are necessary to provide seamless transition of on-chip photons into commercial single-mode optical fibers [39–42].

Herein, we demonstrate on-chip diamond nanophotonics integrated with a high-efficiency fiber-optical interface achieving greater than 90% power coupling at visible wavelengths. Our diamond nanophotonic structures utilize free-standing angled-etched waveguides (Fig. 1), which

*Corresponding author.
loncar@seas.harvard.edu

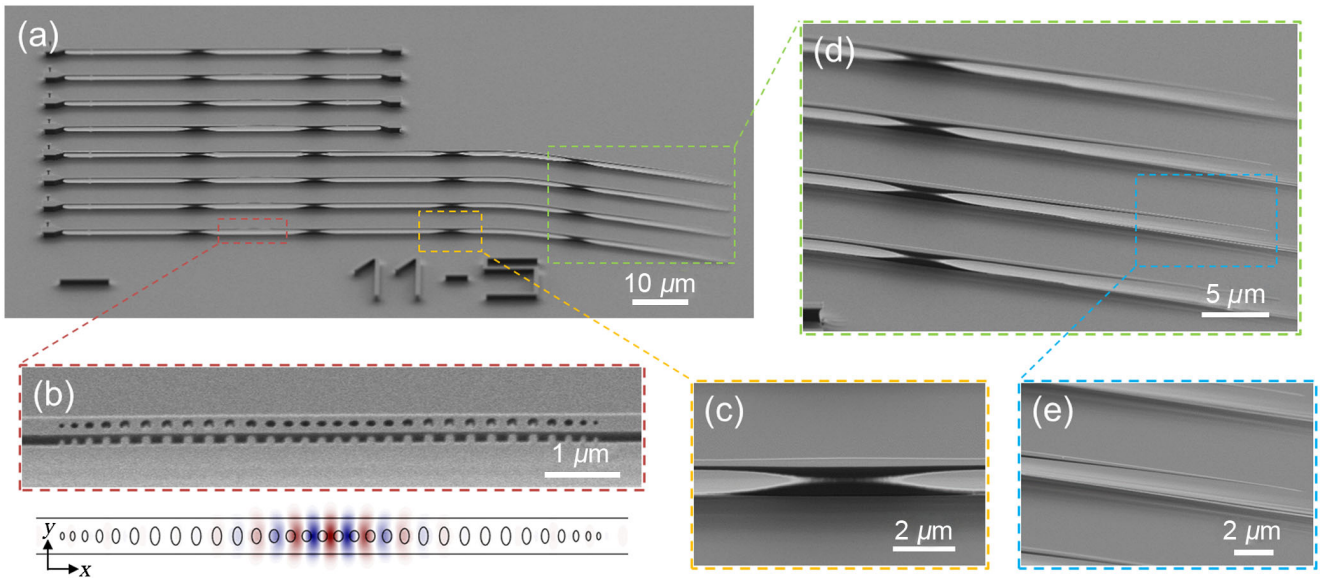

FIG. 1 On-chip diamond nanophotonic structures. SEM images of (a) an array of diamond nanophotonic structures fabricated using angled-etching techniques [45]. The four key components in each device are (1) freestanding diamond waveguides, (2) integrated diamond nanobeam photonic crystal cavities [panels (b) with the top-down electric field profile of the fundamental optical-cavity-mode inset], (3) vertical waveguide support structures [panel (c)], and (4) freestanding diamond waveguide tapers [panels (d) and (e)].

retain low optical loss despite being physically supported through attachment to the bulk substrate [43] and are able to efficiently route photons on chip [31]. The fiber-optical-coupling scheme utilizes a single-mode optical fiber, with one end chemically etched into a conical taper, to adiabatically transition-guided light between on-chip diamond waveguides and off-chip optical-fiber networks. Finally, we use our fiber-coupled diamond nanophotonics platform to demonstrate a bright source of narrow-band single photons (near Fourier limited at <1-GHz bandwidth) based on a SiV center embedded within a waveguide-coupled diamond PCC. We achieve a coherent single-photon generation rate of approximately 38 kHz, representing nearly an order of magnitude improvement compared to previous demonstrations of coherent zero-phonon-line (ZPL) photons collected from a single color center in diamond [5,6,44], with the additional advantage of providing these photons in a single-mode optical fiber. Our work will ultimately enable possibilities for realizing quantum networks that interface multiple emitters, both on chip and separated by long distances.

II. ON-CHIP DIAMOND NANOPHOTONIC STRUCTURES

Figure 1 displays a series of SEM images revealing diamond nanophotonic structures realized by angled-etching nanofabrication [27,28] (see the Supplemental Material [45] for more details). The nanophotonic systems consist of four key components: (1) freestanding diamond waveguides, (2) waveguide-coupled diamond nanobeam photonic crystal cavities [(PCCs) Fig. 1(b)], (3) vertical waveguide support structures [Fig. 1(c)], and (4) freestanding diamond waveguide tapers [(DWTs) Figs. 1(d) and 1(e)].

A. Diamond nanobeam photonic crystal cavities

PCCs enable high optical Q factors while retaining wavelength-scale mode volumes [46], a key ingredient enabling strong light-matter interactions [11,13]. Additionally, diamond nanobeam PCCs [see Fig. 1(b) inset and Ref. [45] for additional details] are readily integrated with on-chip waveguides, as the cavity architecture is naturally built into a suspended waveguide segment. This feature makes it possible to engineer waveguide-damped cavities where decay into the waveguide is much larger than scattering and absorption losses [47,48]. We target the diamond PCC design used in this work to support a fundamental cavity-mode resonance near $\lambda \sim 737$ nm corresponding to the optical transition of the negatively charged SiV center [49,50]. Additionally, we focus on transverse-electric- (TE) polarized cavity modes, which have their major electric field component mostly perpendicular to the $y = 0$ plane [see Fig. 1(b) inset for coordinate convention]. From finite-difference time-domain (FDTD) electromagnetic simulations, the cavity-mode volume is $V_{\mathrm{mode}} \sim 0.52\ (\lambda/n)^3$, where n is the diamond refractive index, a fourfold improvement compared with our previous results for diamond PCCs fabricated in bulk diamond [12], and a twofold improvement over other state-of-the-art systems [21]. For fabricated structures, the number of Bragg mirror segments included in the nanobeam cavity is set to fix the total Q factor of the

device (as confirmed by FDTD simulations) to $Q_{\text{total}} \sim 10^4$, with cavity losses dominated by coupling to the feeding waveguide (intrinsic radiative losses are estimated to be $Q_{\text{rad}} \sim 2 \times 10^5$ by FDTD simulations). Additionally, to limit insertion (scattering) losses into the cavity, several holes that reduce quadratically in pitch and radii are appended to the ends of the PCC to ensure an adiabatic transition between the waveguide mode and Bloch mode of the Bragg mirror [51].

B. Vertical waveguide support structures

Freestanding waveguides and PCCs realized by angled etching ultimately require physical support through attachment to the bulk diamond substrate. To ensure robust mechanical performance while minimizing optical transmission loss, we employ vertical waveguide support structures [43] created by increasing the waveguide width by approximately 30% of the nominal value and gradually tapering over 10-μm-long straight portions [Fig. 1(c)]. With angled-etching nanofabrication, wider waveguide sections require longer etch times to fully release from the bulk substrate. Consequently, wider waveguide sections remain attached to the substrate, resulting in a pedestal-like cross section [31,43]. At the same time, the adiabatically tapered support along the waveguide path minimizes optical transmission losses through the structure. From SEM images, we estimate the thickness of the diamond material supporting the widest portion of the waveguide (midsupport) to be <100 nm, with prior measurements of transmission losses through such fabricated structures to be on the order of approximately 10^{-3} dB per support [31].

C. Diamond waveguide tapers

To efficiently couple light from our diamond nanophotonic structures, we adapt a fiber-optical interface previously developed for suspended silicon nitride nanophotonic systems [39]. Specifically, we employ a single-ended conical optical-fiber taper [(OFT) described in the following section] to make physical contact between the OFT tip and the on-chip freestanding DWT [Fig. 1(e)]. Freestanding DWTs gradually change the effective refractive index of the waveguide mode along the propagation direction, such that nearly all optical power remains in the target eigenmode. To minimize coupling to higher-order modes, we exploit gradual tapering, which fulfills the adiabatic condition [39]: $dn_{\text{wvg}}/dx < (2\pi/\lambda)|n_{\text{eff},1}(x) - n_{\text{eff},2}(x)|^2$, where n_{wvg} is the effective index of the diamond waveguide, $n_{\text{eff},i}$ is the effective index of the ith waveguide mode along the taper, and $\lambda = 737$ nm is the free-space wavelength. Freestanding DWTs are designed to evolve from the nominal diamond waveguide width (approximately 500 nm) down to a <50-nm point, over a 20 μm length, yielding a final taper angle of approximately 2°. We note that the DWTs scale in all three dimensions as a result of angled-etching nanofabrication, since the waveguide width defines its thickness via a constant etch angle [27].

III. EFFICIENT OPTICAL-FIBER TAPER COUPLING

A. Simulation of coupling efficiency

In the region of physical contact between the DWT and OFT [schematically represented in Fig. 2(a)], propagating guided modes couple via their evanescent fields, forming a hybridized "supermode" [39]. Figure 2(b) displays the calculated effective indices of a DWT physically coupled to a single-ended OFT (insets display cross-sectional eigenmode profiles obtained from simulation). With this geometry, the latter supermode has n_{eff} greater than approximately 1.28 over the entire length of the coupler, indicating that the optical mode remains well confined throughout the DWT OFT structure. To confirm adiabatic mode transfer, we employ FDTD simulations to launch a propagating fundamental TE-polarized mode down the diamond waveguide [Fig. 2(c)] and monitor the power output in the HE_{11} optical-fiber mode after the coupling region. A power transfer of approximately 98% is achieved for a 20-μm contact region (equal to the DWT length) corresponding to a coupling loss of less than 0.09 dB per facet. High-efficiency coupling is also observed as the OFT overlap with the DWT is increased up to nearly 50 μm [Fig. 2(c)], while the DWT length is maintained at 20 μm.

B. Optical-fiber taper fabrication

Single-ended conical OFTs are fabricated by a wet-etching technique, where commercial near-infrared single-mode optical fibers (Thorlabs S630-HP) are submerged in hydrofluoric acid (HF) to form the taper profile [52], as depicted in Fig. 2(d). A layer of o-Xylene is added on top of the HF to promote gradual taper formation via an oil-water interface meniscus that wicks up the length of the fiber. As the etch progresses and the fiber diameter shrinks, the height of the oil-water interface meniscus naturally decreases, resulting in a tapered fiber diameter over a length defined by the etch rate and initial fiber diameter. When the acid etches completely through the fiber diameter, the OFT self-terminates. Drawing the fiber out of the HF solution at a fixed rate further extends the taper length, enabling full control over the final taper angle. Moreover, this etching protocol readily extends to the simultaneous fabrication of many nominally identical OFTs. For OFT angles less than 4°, the HE_{11} fiber mode adiabatically transitions over the entire length of the OFT (on the order of 10 mm) [39]. Figure 2(d) shows a SEM image of a representative OFT tip fabricated by HF etching, with a final taper angle of approximately 1.5°. Here, the significant surface roughness of the etched OFT [Fig. 2(e)] is a result of initial surface topography of the original commercial fiber [45]. However,

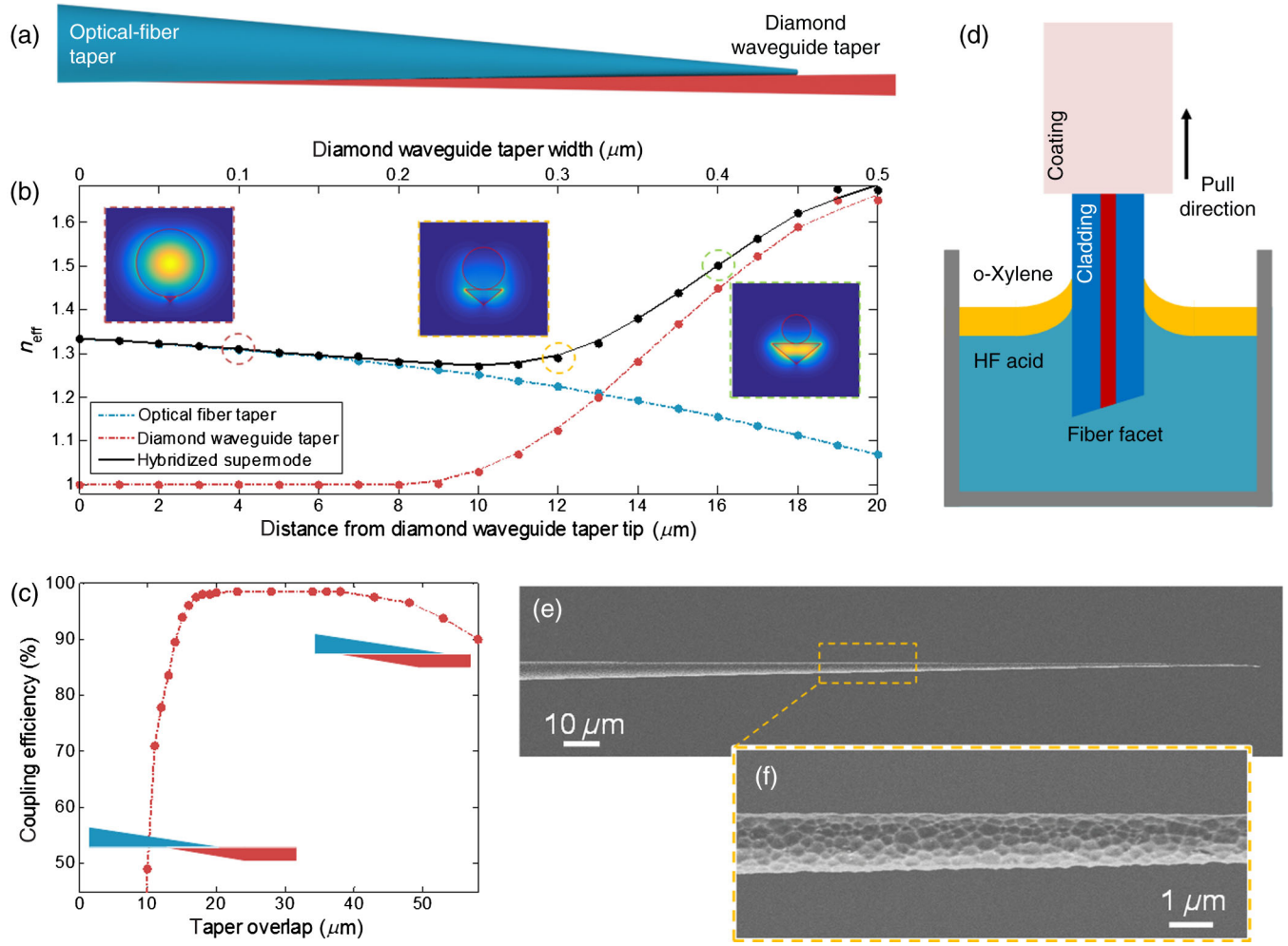

FIG. 2 Single-mode optical-fiber taper fabrication. (a) Schematic of fiber-waveguide taper adiabatic coupling. The single-ended conical OFT (blue) is physically contacted with a DWT (red). (b) Effective indices (n_{eff} calculated via an eigenmode solver) of the OFT and TE-polarized DWT modes for taper angle of 1.5° in both cases. Inset: Cross-sectional energy density profile ($|E|^2$) obtained from eigenmode simulations at the indicated points along the physically overlapped tapers. (c) Simulated coupling efficiencies for transmission from the fundamental diamond TE-polarized waveguide mode to the optical-fiber HE_{11} mode as a function of fiber-waveguide taper overlap for a 20-μm-long DWT. (d) Schematic of the fabrication of single-ended conical OFTs by hydrofluoric acid etching. (e) SEM image of a fabricated OFT tip, with (f) an enlarged image of the chemically etched surface roughness.

the total distance over which the optical mode evanescently leaks outside of the OFT tip is less than approximately 100 μm. Thus, scattering losses due to fiber roughness are not detrimental to the final coupling efficiency.

C. Optical characterization of diamond nanophotonic structures

The generalized optical-fiber network used to collect reflection spectra from the waveguide-coupled diamond PCCs is shown in Fig. 3(a). Motorized stages precisely control the position of the single-ended OFT to bring it into physical contact with the DWT. A white-light laser source (NKT Photonics EXW-12) is coupled into the fiber network and launched into a 2×2 90:10 fiber coupler, with 90% of reflected light returned to the detection path. The transmitted source light polarization is adjusted with an inline fiber polarization controller [(FPC) Thorlabs FPC030) loaded with S630-HP optical fiber to ensure preferential coupling to the fundamental TE-polarized diamond waveguide mode and TE-polarized diamond PCC resonances. Specifically, the diamond waveguide and PCC also support transverse-magnetic- (TM) polarized modes, which spectrally overlap with the TE-polarized modes of interest. For our particular PCC design, a TM passband (high transmission, low reflection) exists in the spectral region associated with the TE stop band (high reflection) and TE-polarized PCC resonances [45]. To avoid leakage of input laser light through coupling to TM-polarized modes, the FPC is adjusted to maximize reflected laser light in the spectral vicinity of the fundamental TE-polarized PCC resonance. Finally, an optical

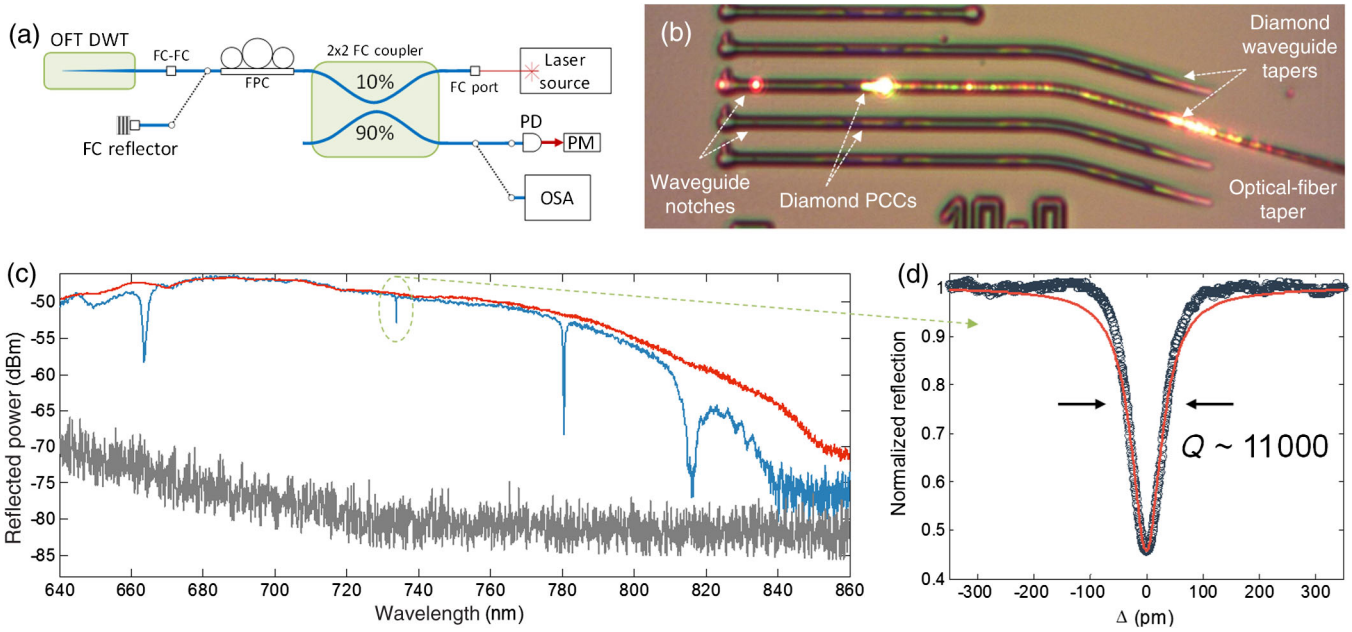

FIG. 3 Optical characterization of diamond nanophotonic structures. (a) Schematic of the visible-band fiber-optical characterization setup. (b) Optical micrograph of a single-ended OFT in contact with a DWT under white-light illumination. (c) Broadband reflection spectra of diamond PCC (blue curve) and a commercial fiber-coupled retroreflector (red curve). The noise floor of the OSA is shown in gray. (d) Normalized high-resolution spectrum of the fundamental diamond nanobeam PCC mode centered at $\lambda \sim 733.9$ nm. A Lorentzian fit (red curve) yields a Q-factor estimate of $Q \sim 1.1 \times 10^4$.

spectrum analyzer (OSA) records the reflection spectra. For a qualitative estimate of the coupling efficiency over a broad wavelength range, the diamond PCC under test is replaced with a commercial fiber-coupled retroreflector (FR-63, Silicon Lightwave Technology, Inc.).

Figure 3(b) displays an optical micrograph of the on-chip diamond nanophotonic network coupled to the OFT tip with the source white-light laser turned on. Light readily couples through the optical-fiber taper tip to the on-chip diamond waveguide, with the diamond PCC acting as a mirror for almost the entire visible emission band. Light passed by the diamond photonic crystal cavity is scattered at the end of the diamond waveguide by an intentionally placed notch in the waveguide. A broadband reflection spectrum collected from a representative diamond PCC [Fig. 3(c), blue curve] exhibits a series of reflection dips attributed to localized TE-polarized cavity resonances and demonstrates the broadband nature (over 200 nm) of this OFT DWT coupling approach. A high-resolution spectrum of the fundamental diamond PCC mode at 733.9 nm (indicated by the green circle) is shown in Fig. 3(d), with a Lorentzian fit to the spectra yielding a Q factor of approximately 1.1×10^4. The on-resonance normalized reflection is approximately 46%, which gives an estimate of the Q factor due to radiative losses or absorption of approximately 3.4×10^4 [48]. Higher-order longitudinal modes of the cavity are strongly waveguide damped; the second-order diamond PCC resonance $\lambda \sim 780$ nm has $Q \sim 1.2 \times 10^3$. We find good agreement between the distribution of observed cavity resonances compared to the design parameters (details provided in Ref. [45]), with a >30% overall yield of PCC devices suitable for experiments described in Sec. IV.

Away from the localized cavity resonances, we assume the diamond PCC ideally reflects all the TE-polarized light coupled to the diamond waveguide, allowing for an accurate calculation of the coupling efficiency. The off-resonant input power (P_{in}) and the reflected powers after the 2×2 coupler (P_r) are measured with a calibrated power meter. The normalized reflection is, thus, given by $P_r/P_{\mathrm{in}} = \eta_c^2 \eta_{\mathrm{BS}} \eta_m \eta_{\mathrm{FC}}$, where η_c is the OFT DWT coupling efficiency, η_{BS} is the calibrated coupling ratio of the 2×2 fiber coupler, η_m is the reflection of the nanobeam cavity Bragg mirror (assumed to be approximately 1), and $\eta_{\mathrm{FC}} \sim 92\%$ is the coupling efficiency of the FC-FC fiber coupler. Neglecting other losses in the diamond waveguide, we estimate a coupling efficiency $\eta_c \sim 91\%$ (measured with a pigtailed laser diode operating at a wavelength of approximately 705 nm). We carry out a series of similar measurements [45] on waveguide-coupled diamond PCCs fabricated for operation at telecom wavelengths (approximately 1480 to 1680 nm). Here, a maximum measured coupling efficiency of approximately 96% demonstrates the broadband nature of both diamond nanophotonics and this adiabatic OFT DWT coupling scheme.

IV. EFFICIENT GENERATION AND COLLECTION OF NARROW-BAND SINGLE PHOTONS

We utilize our described diamond nanophotonic structures to implement a bright source of narrow-band single photons suitable for use in quantum-information protocols. SiV color centers are embedded at the center of waveguide-coupled diamond PCCs via focused-ion-beam (FIB) implantation [12,53,54] followed by high-temperature annealing [45]. Targeted implantation of Si^+ ions by FIB enables the positioning of emitters within the PCC with approximately 40-nm precision in all three dimensions and control over the average number of implanted ions. Substrates in this work include approximately 100 diamond PCCs, each resulting in a suitable SiV-cavity node with accurate spatial alignment. While the conversion yield of implanted Si^+ ions to SiV emitters is approximately 1% to 2%, we implant several hundred ions in each PCC, resulting in several emitters which can be spectrally resolved (due to the native degree of inhomogeneous distribution of the ZPL lines [12]). Therefore, the emitter creation step of our fabrication process is nearly deterministic, with near-unity yield of SiV-cavity nodes suitable for the experiments described below.

SiV centers are excited from free space using a scanning confocal microscope [12]. Fluorescence is detected in the waveguide using the fiber-coupled interface [depicted in Fig. 4(a)]. In order to isolate narrow optical transitions, we cool the device to a temperature of approximately 5 K within a liquid-helium continuous-flow cryostat, at which an optical Λ system formed by the SiV spin-orbit eigenstates is accessible [Fig. 4(b), left inset] [49,50]. We use resonant excitation on the $|u\rangle$-to-$|e\rangle$ branch to generate Raman fluorescence on the $|e\rangle$-to-$|c\rangle$ transition. One benefit of this scheme is that by tuning the frequency of the driving laser, the frequency of the emitted photons can be tuned by more than 10 GHz [12]. We selectively collect this spectral component of the fluorescence using a home-built Fabry-Perot (FP) cavity (finesse approximately 100) as a filter. The intrinsic linewidth of the FP cavity, as measured by a tunable laser, is 1.37 ± 0.05 GHz. This value corresponds to the mean of multiple measurements, where the quoted error represents 1 standard deviation. By scanning the FP cavity center frequency across the $|e\rangle$-to-$|c\rangle$ transition, we measure an upper bound on the linewidth of collected photons of 1.27 ± 0.2 GHz set by the FP cavity [Fig. 4(b)]. This value also represents the mean of all the individual linewidth measurements and its standard

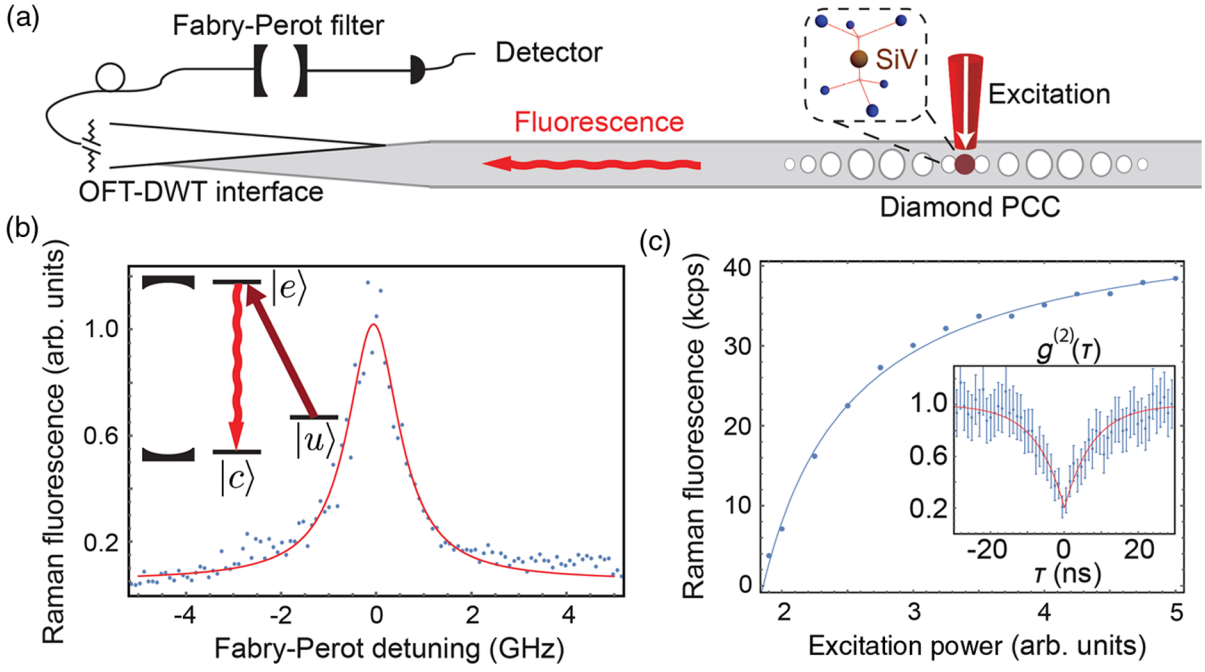

FIG. 4 Efficient generation and collection of narrow-band single photons. (a) A diamond SiV color center embedded inside a diamond PCC is excited from free space, and fluorescence in the diamond waveguide is collected into the optical-fiber taper. A FP cavity is used to measure the spectrum of the emitted photons. (b) Spectrum of collected photons. The excitation laser is resonant with the $|u\rangle$-to-$|e\rangle$ transition. The transmitted Raman fluorescence is recorded as the resonance frequency of the FP cavity is scanned across the $|e\rangle$-to-$|c\rangle$ transition to obtain an upper bound on the linewidth of detected photons of 1.27 ± 0.2 GHz. (c) Saturation measurement of Raman photons with the PCC resonant with the $|e\rangle$-to-$|c\rangle$ transition. We subtract the linear background set by the excitation laser detecting a narrow-band single-photon flux of at least 38 kHz when the PCC is on resonance. Inset: Antibunching of $g^{(2)}(0) = 0.21 \pm 0.09$ in the Raman fluorescence autocorrelation confirms the generation of single photons.

deviation. Given that the linewidth of the SiV Raman fluorescence through the FP cavity is within statistical error of the intrinsic FP cavity linewidth, we conclude that the collected photons are near-Fourier limited with bandwidth significantly less than 1 GHz. Note that the bandwidth of the photons in this Raman scheme is fundamentally limited only by the coherence time of the spin-orbit ground states of the SiV, not the SiV excited-state lifetime [12,55].

With the FP cavity fixed on resonance with the $|e\rangle$-to-$|c\rangle$ transition, we measure the saturation of Raman fluorescence [Fig. 4(c)] when the PCC is tuned onto resonance with the $|e\rangle$-to-$|c\rangle$ transition. Here, κ, the PCC linewidth measured via a tunable laser, is 39 GHz ($Q \sim 10^4$). Tuning of the PCC resonance is achieved via controlled condensation of an inert gas onto the device [12]. We measure a maximum Raman photon detection rate of approximately 38 kHz when the PCC is on resonance. The fluorescence consists of single photons, as confirmed by antibunching in a fluorescence autocorrelation measurement [Fig. 4(c), right inset]. The nonideal $g^2(0)$ value at zero time delay is attributed primarily to leakage of the excitation laser light through the FP cavity, as well as laser-induced background fluorescence. We note that the correlation time of the SiV Raman fluorescence is limited here by a combination of the optical pumping rate and the orbital relaxation time (on the order of 10 ns) [12,55] and not the SiV excited-state lifetime (approximately 1.7 ns).

Our cavity-coupled, coherent photon generation rate represents a significant improvement over the state of the art, when compared against previous demonstrations of coherent ZPL photons collected from a single-diamond color center. The spectral purity (<1-GHz bandwidth) of our collected photons is an essential element of schemes requiring indistinguishable photons, including entanglement generation (the rate of which is typically proportional to the square of the photon generation rate [8]). Our work improves the state of the art for narrow-band photon generation using color centers in diamond, where collection rates for spectrally pure ZPL photons from an individual SiV center [44] or NV center [5,6] of only approximately 6 and 0.2–1.1 kHz were observed, respectively.

Our photon detection rate is limited primarily by finite transmission through the FP cavity filter and related free-space optics (approximately 11% transmission) after collection into the OFT. Accounting for these losses, we estimate a lower bound on the collection rate of unfiltered single photons to be 0.45 MHz in the single-mode optical fiber. Additionally, in the case of the particular Si^+ ion implanted diamond PCC device measured, the OFT DWT coupling efficiency is limited to approximately 22% to 25%, primarily due to mechanical failure of the specific DWTs used in this experiment and the limited degrees of freedom available for accurate fiber positioning in our cryogenic apparatus. We note that the observed mode of failure is a "snapping down" of the DWT into the diamond substrate, which can occur if the sample is air dried out of a solvent. However, sufficient coupling (>10% efficiency) between the OFT and snapped-down DWTs is observed for all devices investigated, giving a near-unity yield for functional DWT creation, with some reaching coupling efficiencies near 40%. While this OFT DWT coupling efficiency is less than what we observe in ambient conditions, typical collection efficiencies into a single-mode fiber are <10% even in the best-case scenario of a high-NA objective and a solid immersion lens machined into the diamond substrate [9] and typically <1%. While recent demonstrations of engineered diamond thin-film gratings (such as bullseye designs [56]) have reported substantially improved photon collection from embedded color centers in bulk systems, our diamond quantum nanophotonic interface provides the additional benefit of an emitter coupled to a well-confined optical mode [12].

Mitigating our current issues with improved postfabrication sample processing and cryogenic OFT-coupling techniques, we expect to increase our detection rate of spectrally filtered ZPL photons beyond the 100-kHz limit, assuming similar transmission losses through the FP cavity filter. Finally, in this continuous-driving Raman scheme, the ultimate limit to the single-photon emission rate is determined by the phonon-limited relaxation time (approximately 40 ns) [55] between the ground states, which is required to reset population into $|u\rangle$ after emission of a Raman photon. In the future, this limitation may be overcome in a pulsed excitation scheme in which the SiV is optically initialized in the state $|u\rangle$ before the Raman excitation pulse is applied.

V. CONCLUSIONS

In summary, we demonstrate on-chip diamond nanophotonic structures with a high-efficiency fiber-optical interface achieving >90% power coupling at visible wavelengths. Our diamond nanophotonic networks utilize freestanding angled-etched waveguides, which retain low optical loss despite being physically supported through attachment to the bulk substrate and are able to efficiently route photons on chip. The fiber-optical coupling utilizes a single-mode optical fiber, with one end chemically etched into a conical taper, to adiabatically transition guided light between on-chip diamond waveguides and off-chip optical-fiber networks. With a SiV center embedded within our waveguide-coupled diamond PCC, we demonstrate an approximately 38-kHz flux of spectrally narrow single photons (<1-GHz bandwidth), efficiently coupled to single-mode optical fiber. Our bright and narrow-band-fiber-integrated diamond nanophotonic quantum node is of immediate technological significance to applications in quantum optics [12]. Combined with advances in quantum control of the diamond SiV center [57–59] and schemes for improved spin-coherence times [55], this platform opens up

possibilities for realizing large-scale systems involving multiple emitters strongly interacting via photons [11,13].

ACKNOWLEDGMENTS

The authors acknowledge V. Venkataraman for useful discussion in the course of preparing this report and D. Perry for performing the focused-ion-beam implantation. This work is supported in part by the AFOSR Quantum Memories MURI (Grant No. FA9550-12-1-0025), ONR MURI on Quantum Optomechanics (Grant No. N00014-15-1-2761), NSF QOP (Grant No. PHY-0969816), NSF CUA (Grant No. PHY-1125846), NSF EFRI ACQUIRE (Grant No. 5710004174), and the STC Center for Integrated Quantum Materials (NSF Grant No. DMR-1231319). Ion implantation is performed with support from the Laboratory Directed Research and Development Program and the Center for Integrated Nanotechnologies at Sandia National Laboratories, an Office of Science facility operated for the DOE (Contract No. DE-AC04-94AL85000) by Sandia Corporation, a Lockheed Martin subsidiary. Device fabrication is performed in part at the Center for Nanoscale Systems, a member of the National Nanotechnology Infrastructure Network, which is supported by the National Science Foundation under Grant No. ECS-0335765. CNS is part of Harvard University.

[1] I. Aharonovich and E. Neu, Diamond nanophotonics, Adv. Opt. Mater. **2**, 911 (2014).

[2] E. Togan, Y. Chu, A. S. Trifonov, L. Jiang, J. Maze, L. Childress, M. V. G. Dutt, A. S. Sorensen, P. R. Hemmer, A. S. Zibrov, and M. D. Lukin, Quantum entanglement between an optical photon and a solid-state spin qubit, Nature (London) **466**, 730 (2010).

[3] L. Childress, M. V. Gurudev Dutt, J. M. Taylor, A. S. Zibrov, F. Jelezko, J. Wrachtrup, P. R. Hemmer, and M. D. Lukin, Coherent dynamics of coupled electron and nuclear spin qubits in diamond, Science **314**, 281 (2006).

[4] M. V. G. Dutt, L. Childress, L. Jiang, E. Togan, J. Maze, F. Jelezko, A. S. Zibrov, P. R. Hemmer, and M. D. Lukin, Quantum register based on individual electronic and nuclear spin qubits in diamond, Science **316**, 1312 (2007).

[5] A. Sipahigil, M. L. Goldman, E. Togan, Y. Chu, M. Markham, D. J. Twitchen, A. S. Zibrov, A. Kubanek, and M. D. Lukin, Quantum Interference of Single Photons from Remote Nitrogen-Vacancy Centers in Diamond, Phys. Rev. Lett. **108**, 143601 (2012).

[6] H. Bernien, L. Childress, L. Robledo, M. Markham, D. Twitchen, and R. Hanson, Two-Photon Quantum Interference from Separate Nitrogen Vacancy Centers in Diamond, Phys. Rev. Lett. **108**, 043604 (2012).

[7] P. C. Maurer, G. Kucsko, C. Latta, L. Jiang, N. Y. Yao, S. D. Bennett, F. Pastawski, D. Hunger, N. Chisholm, M. Markham, D. J. Twitchen, J. I. Cirac, and M. D. Lukin, Room-temperature quantum bit memory exceeding one second, Science **336**, 1283 (2012).

[8] H. Bernien, B. Hensen, W. Pfaff, G. Koolstra, M. S. Blok, L. Robledo, T. H. Taminiau, M. Markham, D. J. Twitchen, L. Childress, and R. Hanson, Heralded entanglement between solid-state qubits separated by three metres, Nature (London) **497**, 86 (2013).

[9] W. Pfaff, B. J. Hensen, H. Bernien, S. B. van Dam, M. S. Blok, T. H. Taminiau, M. J. Tiggelman, R. N. Schouten, M. Markham, D. J. Twitchen, and R. Hanson, Unconditional quantum teleportation between distant solid-state quantum bits, Science **345**, 532 (2014).

[10] B. Hensen, H. Bernien, A. E. Dreau, A. Reiserer, N. Kalb, M. S. Blok, J. Ruitenberg, R. F. L. Vermeulen, R. N. Schouten, C. Abellan, W. Amaya, V. Pruneri, M. W. Mitchell, M. Markham, D. J. Twitchen, D. Elkouss, S. Wehner, T. H. Taminiau, and R. Hanson, Loophole-free Bell inequality violation using electron spins separated by 1.3 kilometres, Nature (London) **526**, 682 (2015).

[11] H. J. Kimble, The quantum internet, Nature (London) **453**, 1023 (2008).

[12] A. Sipahigil, R. E. Evans, D. D. Sukachev, M. J. Burek, J. Borregaard, M. Bhaskar, C. Nguyen, J. Pacheco, H. A. Atikian, C. Meuwly, R. M. Camacho, F. Jelezko, E. Bielejec, H. Park, M. Loncar, and M. D. Lukin, An integrated diamond nanophotonics platform for quantum-optical networks, Science **354**, 847 (2016).

[13] D. E. Chang, V. Vuletic, and M. D. Lukin, Quantum nonlinear optics–photon by photon, Nat. Photonics **8**, 685 (2014).

[14] B. J. M. Hausmann, B. J. Shields, Q. Quan, Y. Chu, N. P. de Leon, R. Evans, M. J. Burek, A. S. Zibrov, M. Markham, D. J. Twitchen, H. Park, M. D. Lukin, and M. Lončăr, Coupling of NV centers to photonic crystal nanobeams in diamond, Nano Lett. **13**, 5791 (2013).

[15] B. J. M. Hausmann, I. B. Bulu, P. B. Deotare, M. McCutcheon, V. Venkataraman, M. L. Markham, D. J. Twitchen, and M. Lončar, Integrated high-quality factor optical resonators in diamond, Nano Lett. **13**, 1898 (2013).

[16] A. Faraon, C. Santori, Z. Huang, V. M. Acosta, and R. G. Beausoleil, Coupling of Nitrogen-Vacancy Centers to Photonic Crystal Cavities in Monocrystalline Diamond, Phys. Rev. Lett. **109**, 033604 (2012).

[17] A. Faraon, P. E. Barclay, C. Santori, K.-M. C. Fu, and R. G. Beausoleil, Resonant enhancement of the zero-phonon emission from a colour centre in a diamond cavity, Nat. Photonics **5**, 301 (2011).

[18] A. Faraon, C. Santori, Z. Huang, K.-M. C. Fu, V. M. Acosta, D. Fattal, and R. G. Beausoleil, Quantum photonic devices in single-crystal diamond, New J. Phys. **15**, 025010 (2013).

[19] J. C. Lee, D. O. Bracher, S. Cui, K. Ohno, C. A. McLellan, X. Zhang, P. Andrich, B. Alemán, K. J. Russell, A. P. Magyar, I. Aharonovich, A. Bleszynski Jayich, D. Awschalom, and E. L. Hu, Deterministic coupling of delta-doped nitrogen vacancy centers to a nanobeam photonic crystal cavity, Appl. Phys. Lett. **105**, 261101 (2014).

[20] A. P. Magyar, J. C. Lee, A. M. Limarga, I. Aharonovich, F. Rol, D. R. Clarke, M. Huang, and E. L. Hu, Fabrication of thin, luminescent, single-crystal diamond membranes, Appl. Phys. Lett. **99**, 081913 (2011).

[21] L. Li, T. Schröder, E. H. Chen, M. Walsh, I. Bayn, J. Goldstein, O. Gaathon, M. E. Trusheim, M. Lu, J. Mower, M. Cotlet, M. L. Markham, D. J. Twitchen, and D. Englund, Coherent spin control of a nanocavity-enhanced qubit in diamond, Nat. Commun. **6**, 6173 (2015).

[22] M. K. Bhaskar, D. D. Sukachev, A. Sipahigil, R. E. Evans, M. J. Burek, C. T. Nguyen, L. J. Rogers, P. Siyushev, M. H. Metsch, H. Park, F. Jelezko, M. Loncar, and M. D. Lukin, Quantum Nonlinear Optics with a Germanium-Vacancy Color Center in a Nanoscale Diamond Waveguide, Phys. Rev. Lett. **118**, 223603 (2017).

[23] J. C. Lee, I. Aharonovich, A. P. Magyar, F. Rol, and E. L. Hu, Coupling of silicon-vacancy centers to a single crystal diamond cavity, Opt. Express **20**, 8891 (2012).

[24] J. Riedrich-Moller, L. Kipfstuhl, C. Hepp, E. Neu, C. Pauly, F. Mucklich, A. Baur, M. Wandt, S. Wolff, M. Fischer, S. Gsell, M. Schreck, and C. Becher, One- and two-dimensional photonic crystal microcavities in single crystal diamond, Nat. Nanotechnol. **7**, 69 (2012).

[25] J. Riedrich-Möller, C. Arend, C. Pauly, F. Mücklich, M. Fischer, S. Gsell, M. Schreck, and C. Becher, Deterministic coupling of a single silicon-vacancy color center to a photonic crystal cavity in diamond, Nano Lett. **14**, 5281 (2014).

[26] S. Mouradian, N. H. Wan, T. Schröder, and D. Englund, Rectangular photonic crystal cavities in bulk diamond, Appl. Phys. Lett. **111**, 021103 (2017).

[27] M. J. Burek, N. P. de Leon, B. J. Shields, B. J. M. Hausmann, Y. Chu, Q. Quan, A. S. Zibrov, H. Park, M. D. Lukin, and M. Lončar, Free-standing mechanical and photonic nanostructures in single-crystal diamond, Nano Lett. **12**, 6084 (2012).

[28] P. Latawiec, M. J. Burek, Y.-I. Sohn, and M. Lončar, Faraday cage angled-etching of nanostructures in bulk dielectrics, J. Vac. Sci. Technol. B **34**, 041801 (2016).

[29] H. A. Atikian, P. Latawiec, M. J. Burek, Y.-I. Sohn, S. Meesala, N. Gravel, A. B. Kouki, and M. Lončar, Free-standing nanostructures via reactive ion beam angled etching, APL Photonics **2**, 051301 (2017).

[30] I. Bayn, S. Mouradian, L. Li, J. A. Goldstein, T. Schröder, J. Zheng, E. H. Chen, O. Gaathon, M. Lu, A. Stein, C. A. Ruggiero, J. Salzman, R. Kalish, and D. Englund, Fabrication of triangular nanobeam waveguide networks in bulk diamond using single-crystal silicon hard masks, Appl. Phys. Lett. **105**, 211101 (2014).

[31] M. J. Burek, Y. Chu, M. S. Z. Liddy, P. Patel, J. Rochman, S. Meesala, W. Hong, Q. Quan, M. D. Lukin, and M. Lončar, High quality-factor optical nanocavities in bulk single-crystal diamond, Nat. Commun. **5**, 5718 (2014).

[32] R. E. Evans, A. Sipahigil, D. D. Sukachev, A. S. Zibrov, and M. D. Lukin, Narrow-Linewidth Homogeneous Optical Emitters in Diamond Nanostructures via Silicon Ion Implantation, Phys. Rev. Applied **5**, 044010 (2016).

[33] Y. Chu, N. P. de Leon, B. J. Shields, B. Hausmann, R. Evans, E. Togan, M. J. Burek, M. Markham, A. Stacey, A. S. Zibrov, A. Yacoby, D. J. Twitchen, M. Loncar, H. Park, P. Maletinsky, and M. D. Lukin, Coherent optical transitions in implanted nitrogen vacancy centers, Nano Lett. **14**, 1982 (2014).

[34] P. Latawiec, V. Venkataraman, M. J. Burek, B. J. M. Hausmann, I. Bulu, and M. Lončar, On-chip diamond Raman laser, Optica **2**, 924 (2015).

[35] B. J. M. Hausmann, I. Bulu, V. Venkataraman, P. Deotare, and M. Loncar, Diamond nonlinear photonics, Nat. Photonics **8**, 369 (2014).

[36] M. J. Burek, J. D. Cohen, S. M. Meenehan, N. El-Sawah, C. Chia, T. Ruelle, S. Meesala, J. Rochman, H. A. Atikian, M. Markham, D. J. Twitchen, M. D. Lukin, O. Painter, and M. Lončar, Diamond optomechanical crystals, Optica **3**, 1404 (2016).

[37] M. Mitchell, B. Khanaliloo, D. P. Lake, T. Masuda, J. P. Hadden, and P. E. Barclay, Single-crystal diamond low-dissipation cavity optomechanics, Optica **3**, 963 (2016).

[38] S. L. Mouradian, T. Schröder, C. B. Poitras, L. Li, J. Goldstein, E. H. Chen, M. Walsh, J. Cardenas, M. L. Markham, D. J. Twitchen, M. Lipson, and D. Englund, Scalable Integration of Long-Lived Quantum Memories into a Photonic Circuit, Phys. Rev. X **5**, 031009 (2015).

[39] T. G. Tiecke, K. P. Nayak, J. D. Thompson, T. Peyronel, N. P. de Leon, V. Vuletić, and M. D. Lukin, Efficient fiber-optical interface for nanophotonic devices, Optica **2**, 70 (2015).

[40] S. Gröblacher, J. T. Hill, A. H. Safavi-Naeini, J. Chan, and O. Painter, Highly efficient coupling from an optical fiber to a nanoscale silicon optomechanical cavity, Appl. Phys. Lett. **103**, 181104 (2013).

[41] R. S. Daveau, K. C. Balram, T. Pregnolato, J. Liu, E. H. Lee, J. D. Song, V. Verma, R. Mirin, S. W. Nam, L. Midolo, S. Stobbe, K. Srinivasan, and P. Lodahl, Efficient fiber-coupled single-photon source based on quantum dots in a photonic-crystal waveguide, Optica **4**, 178 (2017).

[42] R. N. Patel, T. Schroder, N. Wan, L. Li, S. L. Mouradian, E. H. Chen, and D. R. Englund, Efficient photon coupling from a diamond nitrogen vacancy center by integration with silica fiber, Light Sci. Appl. **5**, e16032 (2016).

[43] M. J. Burek and M. Loncar, Device support structures from bulk substrates, U.S. Patent App. No. 13/954,108 (5, February, 2015).

[44] A. Sipahigil, K. D. Jahnke, L. J. Rogers, T. Teraji, J. Isoya, A. S. Zibrov, F. Jelezko, and M. D. Lukin, Indistinguishable Photons from Separated Silicon-Vacancy Centers in Diamond, Phys. Rev. Lett. **113**, 113602 (2014).

[45] See Supplemental Material at http://link.aps.org/supplemental/10.1103/PhysRevApplied.8.024026 for additional details of fabrication, device simulations, and optical measurements.

[46] P. B. Deotare, M. W. McCutcheon, I. W. Frank, M. Khan, and M. Lončar, High quality factor photonic crystal nanobeam cavities, Appl. Phys. Lett. **94**, 121106 (2009).

[47] Q. Quan, P. B. Deotare, and M. Loncar, Photonic crystal nanobeam cavity strongly coupled to the feeding waveguide, Appl. Phys. Lett. **96**, 203102 (2010).

[48] J. D. Joannopoulos, S. G. Johnson, J. N. Winn, and R. D. Meade, *Photonic Crystals: Molding the Flow of Light*, 2nd ed. (Princeton University Press, Princeton, NJ, 2008).

[49] L. J. Rogers, K. D. Jahnke, M. W. Doherty, A. Dietrich, L. P. McGuinness, C. Müller, T. Teraji, H. Sumiya, J. Isoya, N. B. Manson, and F. Jelezko, Electronic structure of the

negatively charged silicon-vacancy center in diamond, Phys. Rev. B **89**, 235101 (2014).

[50] C. Hepp, T. Müller, V. Waselowski, J. N. Becker, B. Pingault, H. Sternschulte, D. Steinmüller-Nethl, A. Gali, J. R. Maze, M. Atatüre, and C. Becher, Electronic Structure of the Silicon Vacancy Color Center in Diamond, Phys. Rev. Lett. **112**, 036405 (2014).

[51] C. Sauvan, G. Lecamp, P. Lalanne, and J. P. Hugonin, Modal-reflectivity enhancement by geometry tuning in photonic crystal microcavities, Opt. Express **13**, 245 (2005).

[52] D. R. Turner, Etch procedure for optical fibers, U.S. Patent No. 4,469,554 (4, September, 1984).

[53] T. Schröder, M. E. Trusheim, M. Walsh, L. Li, J. Zheng, M. Schukraft, J. L. Pacheco, R. M. Camacho, E. S. Bielejec, A. Sipahigil, R. E. Evans, D. D. Sukachev, C. T. Nguyen, M. D. Lukin, and D. Englund, Scalable focused ion beam creation of nearly lifetime-limited single quantum emitters in diamond nanostructures, Nat. Commun. **8**, 15376 (2017).

[54] T. Syuto, K. Godai, K. Akira, T. Tokuyuki, O. Shinobu, P. M. Liam, R. Lachlan, N. Boris, E. Wu, Y. Liu, J. Fedor, O. Takeshi, I. Junichi, S. Takahiro, and T. Takashi, Array of bright silicon-vacancy centers in diamond fabricated by low-energy focused ion beam implantation, Appl. Phys. Express **7**, 115201 (2014).

[55] K. D. Jahnke, A. Sipahigil, J. M. Binder, M. W. Doherty, M. Metsch, L. J. Rogers, N. B. Manson, M. D. Lukin, and F. Jelezko, Electron-phonon processes of the silicon-vacancy centre in diamond, New J. Phys. **17**, 043011 (2015).

[56] L. Li, E. H. Chen, J. Zheng, S. L. Mouradian, F. Dolde, T. Schröder, S. Karaveli, M. L. Markham, D. J. Twitchen, and D. Englund, Efficient photon collection from a nitrogen vacancy center in a circular bullseye grating, Nano Lett. **15**, 1493 (2015).

[57] J. N. Becker, J. Görlitz, C. Arend, M. Markham, and C. Becher, Ultrafast all-optical coherent control of single silicon vacancy colour centres in diamond, Nat. Commun. **7**, 13512 (2016).

[58] L. J. Rogers, K. D. Jahnke, M. H. Metsch, A. Sipahigil, J. M. Binder, T. Teraji, H. Sumiya, J. Isoya, M. D. Lukin, P. Hemmer, and F. Jelezko, All-Optical Initialization, Readout, and Coherent Preparation of Single Silicon-Vacancy Spins in Diamond, Phys. Rev. Lett. **113**, 263602 (2014).

[59] B. Pingault, J. N. Becker, C. H. H. Schulte, C. Arend, C. Hepp, T. Godde, A. I. Tartakovskii, M. Markham, C. Becher, and M. Atatüre, All-Optical Formation of Coherent Dark States of Silicon-Vacancy Spins in Diamond, Phys. Rev. Lett. **113**, 263601 (2014).